ISSN 1070-3284, Russian Journal of Coordination Chemistry, 2016, Vol. 42, No. 6, pp. 392–401. © Pleiades Publishing, Ltd., 2016.

Experimental and Computational Studies of [N'-(2-Hydroxy-3-Methoxybenzylidene)-4-Methylbenzenesulfonohydrazide]nickel(II)[1]

N. Şenyüz[a], Ç. Yüksektepe Ataol[b, *], F. Güntepe[c], H. Bati[a], and M. Taş[d]

[a] *Department of Chemistry, Faculty Arts and Sciences, Ondokuz Mayis University, Kurupelit, Samsun, 55139 Turkey*
[b] *Department of Physics, Faculty of Science, Cankiri Karatekin University, Uluyazi, Cankiri, 18100 Turkey*
[c] *Department of Physics, Faculty of Science, Ondokuz Mayis University, Kurupelit, Samsun, 55139 Turkey*
[d] *Department of Science Education, Faculty of Education, Ondokuz Mayis University, Kurupelit, Samsun, 55139 Turkey*
**e-mail: yuksektepe.c@karatekin.edu.tr; yuksekc85@gmail.com*

Received July 2, 2015

Abstract—Mononuclear Ni(II) complex ($C_{30}H_{30}NiN_4O_8S_2$) (**I**) has been obtained with 1 : 2 metal/ligand ratio and characterized by single crystal X-ray diffraction (CIF file CCDC no. 1040830), IR, UV-Vis spectroscopic techniques and DFT. X-ray results show that complex **I** crystallizes in the monoclinic system, space group $P2_1/n$ with four molecules in the unit cell. In structure **I**, the coordination around Ni atom is distorted square planar. In addition to the crystal structure, the molecular geometry, vibrational frequencies, molecular electrostatic potential, and frontier molecular orbital analysis of compound **I** in the ground state have been calculated using the B3LYP/6-311G and B3LYP/3-21G methods. The computed vibrational frequencies are used to determine the types of molecular motions associated with each of the observed experimental bands.

DOI: 10.1134/S1070328416060063

INTRODUCTION

Many Schiff base complexes have potential biological interest in an attempt to mimic the structural and functional features of multimetal active sites. Schiff bases are also found useful applications in the synthesis of molecular and supramolecular polymetallic functional systems exhibiting specific optical or magnetic properties [1]. Schiff bases constitute an interesting class of chelating agents, capable of coordination with one or more metal ions to form mononuclear as well as polynuclear metal complexes [2, 3]. Some of their applications can be found in analytical chemistry and serve as biochemical models [4, 5]. Most Schiff bases have antibacterial, anticancer, anti-inflammatory and antitoxic activities [6]; in particular, sulfur-containing Schiff bases are very effective. Schiff bases have played an important role in the devolopment coordination chemistry and Schiff bases ligands are well known their wide range of application in pharmaceutical and industrial field [7, 8]. The coordination compounds derived from Schiff bases with transition metals have been studied with wide scope of their applications [9].

Hydrazones are used as intermediates in synthesis [10], as functional groups in metal carbonyls [11], in organic compounds [12, 13] and in particular in hydrazone Schiff base ligands [14–17], which are among others employed in dinuclear catalysts [18]. Furthermore, hydrazones exhibit physiological activities in the treatment of several diseases such as tuberculosis. This activity is attributed to the formation of stable chelate complexes with transition metals which catalyze physiological processes [19–21]. In analytical chemistry hydrazones find applications as multidentate ligands for transition metals in colorimetric or fluorimetric determinations [22, 23].

We have prepared a new sulfonohydrazide Ni(II) complex—[N'-(2-hydroxy-3-methoxybenzylidene)-4-methylbenzenesulfonohydrazide]nickel(II) ($C_{30}H_{30}NiN_4O_8S_2$) (**I**) which has been identified by a combination of FT-IR spectra, UV-Vis spectra, magnetic susceptibility measurements, and single crystal X-ray diffraction. Molecular structure, vibrational assignments, frontier molecular orbital analysis, and molecular electrostatic potential (MEP) of bidentate transition metal complexes in the ground state have been investigated using density functional theory (DFT/B3LYP). The first aim of this study is to understand its crystal and molecular structures by X-ray analysis and quantum chemical method, comparing experimental, and theoretical results. The chemical diagram of **I** is the following:

[1] The article is published in the original.

Table 1. Crystallographic data and structure refinement for complex **I**

Parameter	Value
Empirical formula	$C_{30}H_{30}N_4O_8S_2Ni$
Fw	697.4
Crystal system	Monoclinic
Space group	$P2_1/n$
Unit cell dimensions:	
a, Å	8.953(5)
b, Å	21.044(5)
c, Å	16.505(5)
β, deg	93.969(5)
Volume, Å^3	3102.20(24)
Z	4
ρ_{calcd}, mg m^{-3}	1.49
μ, mm^{-1}	0.817
Aborption correction	Multi-scan
Diffractometer/measurement	SuperNova (Single source at offset), Eos diffractometer/rotation (ω scan)
Index ranges (*h, k, l*)	$-10 \leqslant h \leqslant 6$, $-14 \leqslant k \leqslant 25$, $-16 \leqslant l \leqslant 19$
θ Range for data collection, deg	3.14–32.20
Reflections collected	11897
Independent reflections	5299
Observed reflections ($I > 2\sigma(I)$)	2929
R_{int}	0.072
Goodness-of-fit on F^2	0.862
Final *R* indices ($I > 2\sigma(I)$)	$R_1 = 0.053$, $wR_2 = 0.097$
$\Delta\rho_{max}$, $\Delta\rho_{min}$, *e* Å^{-3}	0.368, −0.394
Extinction coefficient	0.0009

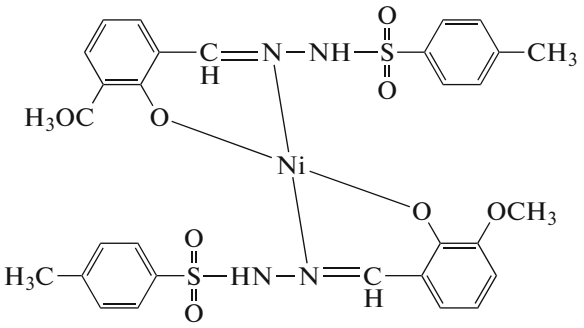

EXPERIMENTAL

Physical measurements and theoretical methods. The optical absorption spectra of complex **I** were recorded at room temperature in acetonitrile solution on a Unicam UV2 UV-Vis spectrometer working between 200 and 900 nm. IR spectra were recorded on a Vertex 80v Bruker FTIR spectrophotometer in 4000–400 cm^{-1} using KBr pellets.

Starting geometries of compound I were taken from X-ray refinement data. The molecular structures of compound I in the ground state (*in vacuo*) were optimized by DFT methods to include correlation corrections with the 3-21G and 6-311G basis sets. In DFT calculations, hybrid functionals are also used, including the Becke's three-parameter functional (B3) [24], which defines the exchange functional as the linear combination of Hartree–Fock, local, and gradient-corrected exchange terms. The B3 hybrid functional was used in combination with the correlation functionals [25].

Then vibrational frequencies for optimized molecular structures have been calculated. Besides of this, the lowest unoccupied molecular orbital (LUMO) highest occupied molecular orbital (HOMO) energy differences were calculated with time-dependent density functional theory (TD-DFT). All the calculations were performed using the Gaussview molecular visualization program [26] and Gaussian 03 program on a personal computer [27].

Synthesis of complex I. An ethanolic solution (15 mL) of *o*-vanillin (2 mmol, 0.304 g) was added to a solution of 4-methylbenzenesulfonylhydrazine (2 mmol, 0.372 g), in ethanol (15 mL). There sulting solution was stirred for half an hour, and then $Ni(CH_3COO)_2 \cdot 6H_2O$ (1 mmol, 0.285 g) in 10 mL ethanol was added. The solution was refluxed for 48 h with stirring. The mixture was then cooled to room temperature and a brown powder was precipitated. The product was filtered and washed with ethanol. Crystals of suitable for X-ray diffraction were grown from acetonitrille–chloroform (1 : 1) solution by slow evaporation over a period of 6 days (m.p.: 227°C and yield 65%).

X-ray crystallography. Data collection was carried out on a Oxford Diffraction SuperNova (single source at offset) Eos diffractometer equipped with a graphite monochromated MoK_α radiation (λ = 0.7107 Å) at 293 K. The structure was solved by direct methods using SHELXS-97 [28] implemented in the WinGX software system [29] and refined by full-matrix least-squares procedure on F^2 using SHELXL-97 [28]. All non-hydrogen atoms were easily found from the difference Fourier map and refined anisotropically. All hydrogen atoms were included using a riding model and refined isotropically with C–H = 0.93–0.97 and N–H = 0.86 Å. $U_{iso}(H) = 1.2U_{eq}(C, N)$, $U_{iso}(H) = 1.5U_{eq}$ (for methyl group). Crystals of **I** were found approximately 0.25 : 0.75 ratio to be twinned. The crystal was a non-morehedral twin crystal with two

Table 2. Selected geometrical parameters of **I** with X-ray structure and the DFT method

Bond	Experimental	B3LYP 3-21G	B3LYP 6-311G
	d, Å		
Ni–O(1)	1.825(2)	1.7663	1.8336
Ni–O(2)	1.825(3)	1.7658	1.8335
Ni–N(2)	1.897(3)	1.8289	1.9101
Ni–N(3)	1.893(3)	1.8289	1.9102
S(1)–O(5)	1.427(3)	1.5889	1.6351
S(1)–O(6)	1.423(3)	1.5945	1.6400
S(1)–N(1)	1.660(3)	1.8977	2.0088
S(2)–O(7)	1.425(3)	1.5942	1.6400
S(2)–O(8)	1.425(3)	1.5888	1.6351
S(2)–N(4)	1.676(3)	1.5945	2.0091
N(1)–N(2)	1.420(4)	1.4640	1.4056
N(3)–N(4)	1.421(4)	1.4648	1.4056
N(2)–C(1)	1.293(5)	1.3234	1.3269
N(3)–C(16)	1.299(5)	1.3236	1.3270
Bond angle		deg	
N(2)NiN(3)	179.07(15)	174.82	180.00
O(1)NiN(2)	92.57(13)	92.20	92.51
O(2)NiN(3)	92.84(13)	92.09	92.50
O(1)NiO(2)	177.91(12)	177.64	180.00
O(2)NiN(2)	87.17(13)	87.85	87.49
O(1)NiN(3)	87.46(13)	88.07	87.49
O(5)S(1)O(6)	120.61(19)	120.88	123.09
O(5)S(1)N(1)	103.27(18)	105.52	105.15
O(6)S(1)N(1)	107.37(18)	105.47	102.82
O(7)S(2)O(8)	120.53(19)	121.02	123.10
O(7)S(2)N(4)	107.29(19)	105.53	102.81
O(8)S(2)N(4)	103.79(19)	105.74	105.17
C(16)N(3)Ni	125.6(3)	129.06	126.63
C(1)N(2)Ni	125.7(3)	129.03	126.63
C(18)O(2)Ni	128.6(3)	132.43	130.96
C(7)O(1)Ni	126.3(2)	132.01	130.96
C(1)N(2)N(1)	115.7(3)	111.71	113.75
C(16)N(3)N(4)	115.8(3)	111.65	113.75
N(1)N(2)Ni	118.6(2)	119.24	119.60
N(4)N(3)Ni	118.5(3)	119.24	119.60
N(2)N(1)S(1)	114.0(2)	108.85	110.28
N(3)N(4)S(2)	112.6(2)	108.57	110.26
Torsion angles		deg	
O(1)NiN(3)N(4)	−18.4(2)	0.42	−0.01
O(2)NiN(3)N(4)	159.5(2)	−177.22	180.00
N(2)NiN(3)N(4)	−110.0(10)	93.56	147.66
O(1)NiN(2)C(1)	17.4(3)	1.08	1.73
O(2)NiN(2)C(1)	−160.5(3)	178.72	−178.28
N(3)NiN(2)C(1)	109.0(10)	−91.88	−145.94
O(1)NiN(2)N(1)	−161.7(2)	179.52	179.98
O(2)NiN(2)N(1)	20.4(3)	−2.83	−0.03
N(3)NiN(2)N(1)	−70.0(10)	86.57	32.31
O(2)NiO(1)C(7)	56.0(3)	−97.78	−120.67

reciprocal lattice differently oriented giving rise to double diffraction spot sets. Reflection data were measured for the two twin domains, scaled and combined together, but overlapping reflections could not be satisfactorily measured and were discarded, leading to a data completeness of about 97%. Data collection,

CrysAlisPro [30]; cell refinement, CrysAlisPro; data reduction, CrysAlisPro. The molecular structure plots were prepared by using the ORTEP III for Windows [31]. Crystallographic data, details of the data collection and structure refinements are listed in Table 1, the selected geometric parameters are given in Table 2.

Supplementary material for structure **I** has been deposited with the Cambridge Crystallographic Data Centre (no. 1040830; deposit@ccdc.cam.ac.uk or http://www.ccdc.cam.ac.uk).

RESULTS AND DISCUSSION

The X-ray structure of **I** was determined in order to confirm the assigned structure and to establish conformation of the molecule. ORTEP drawing of the structure with atomic numbering is shown in Fig. 1a. Complex **I** is centrosymmetric where Ni atom is coordinated to two sulfonylhydrazide ligands via hydrazone nitrogens (N(2) and N(3)) and hydroxyl O(1) and O(2) atoms. The ligand : metal ratio was 2 : 1 in the case of complex **I**. The coordination around Ni atom is distorted square planar. Deviation from idealized square planar arrengement evident from the values of both *cis*- and *trans* bond angles arround the central Ni atom in Table 2. The Ni–N(2)–O(2)–N(3)–O(1) atoms is nearly planar with a mean deviation of 0.0260(14) Å for O(1). The dihedral angle between the coordination Ni–N(2)–O(2)–N(3)–O(1) and C(2)–C(7) planes is 22.00(16)° while the C(9)–C(14) deviate from the Ni coordination plane by 18.37(17)°. The C(17)–C(22) and C(24)–C(29) planes also form dihedral angles of 33.86(15)° and 24.06(16)° with the Ni coordination plane, respectively. As can be seen in [32], the C–S–N(H)–N sulfonohydrazide linkage is non-planar; the torsion angles are −52.5° and 57.8° for C(9)–S(1)–N(1H)–N(2) and C(24)–S(2)–N(4H)–N(3), respectively, the S atom showing a tetrahedral environment suggests a sp^3 hybridization for the S atom. The C–N bond lengths in compound **I** are 1.293(5) and 1.299 (5) Å for N(2)–C(1) and N(3)–C(16), respectively, which shorter than a C–N single bond length 1.443 Å [33], but longer than a typical C=N bond length 1.269 Å [34], indicating delocalization.

In the molecular structure of compound **I**, it is observed that the sulfonyl oxygens O(6) and O(8) involved in intramolecular hydrogen bonds with the C(14)–H and C(29)–H protons, respectively (Fig. 1a). These hydrogen bonds motif of graph set descriptors S(5) form five membered rings. Despite the compound contains a lot of potential donor-acceptor sites, there is no classic hydrogen bond is observed. The sulfonyl oxygen O(8) is involved in C–H···O weak hydrogen bond formation with the C(3)–H proton at $1 + x, y, z$. This hydrogen bond of graph set descriptor C(10) [35] forms a chain propagating along the x axis as shown in Fig. 2. Also, in the crystals packing, the weak C–H···π or π···ring interactions are effective. The details of hydrogen bonds are given in Table 3.

The optimized molecular structure of **I** is shown in Fig. 1b. Some selected geometric parameters experimentally obtained and theoretically calculated by B3LYP/3-21G and B3LYP/6-311G methods are listed in Table 2. Experimental results are solid phase and theoretical calculations are gaseous phase. In the solid state, intermolecular interactions connect molecules, resulting in differences of bond parameters between calculated and experimental values. DFT optimized geometric parameters are usually in good agreement with experimental values and more accurate than Hartree–Fock and semi-empirical methods, due to inclusion of electron correlation.

The largest differences between experimental and calculated bond lengths, bond angles and torsion angles are 0.238 and 0.349 Å, 5.71° and 4.66°, 41.78°, and 64.67° for B3LYP/3-21G and B3LYP/6-311G, respectively. Optimized bond lengths and torsion angles provided by B3LYP/3-21G method are the closest to the experimental values (Table 2) whereas the dihedral angles are provided by B3LYP/6-311G show the best agreement with the experimental values.

Vibrational frequencies are calculated at the B3LYP/3-21G and B3LYP/6-311G levels for **I**. Some primary calculated harmonic frequencies are listed in Table 4 and compared with experimental data; assignments are also indicated in Table 4. Gaussview molecular visualization program was used to assign the calculated harmonic frequencies. IR spectra of **I** has been studied to characterize its structure.

In the experimental IR spectrum of complex **I**, a sharp band observed at 3101 cm^{-1} is assigned to the ν(NH) group. The characteristic phenolic ν(OH), due to the presence of an hydroxy group at the *o*-position, was observed in ligand at 3148 cm^{-1}. In IR spectrum of the complex **I**, these ν(OH) peaks have disappeared after deprotonation, and the phenolic oxygen coordinats with the Ni atom. However, such coordination is supported by the shifting of the phenolic ν(C–O) to lower wavenumber in the complex. In IR spectra of the Schiff base ligand, a sharp band at 1610 cm^{-1} is assigned to the ν(C=N) mode of the azomethine group. These shifts to lower wavenumbers in NiL complex suggest the coordination of the azomethine nitrogen to the Ni atom. This is further substantiated by the presence of a new band at 445 cm^{-1} is assigned to ν(M–N). In IR spectrum of complex, the two bands at 1318, 1166 cm^{-1} are attributed to $\nu_s(SO_2)$,

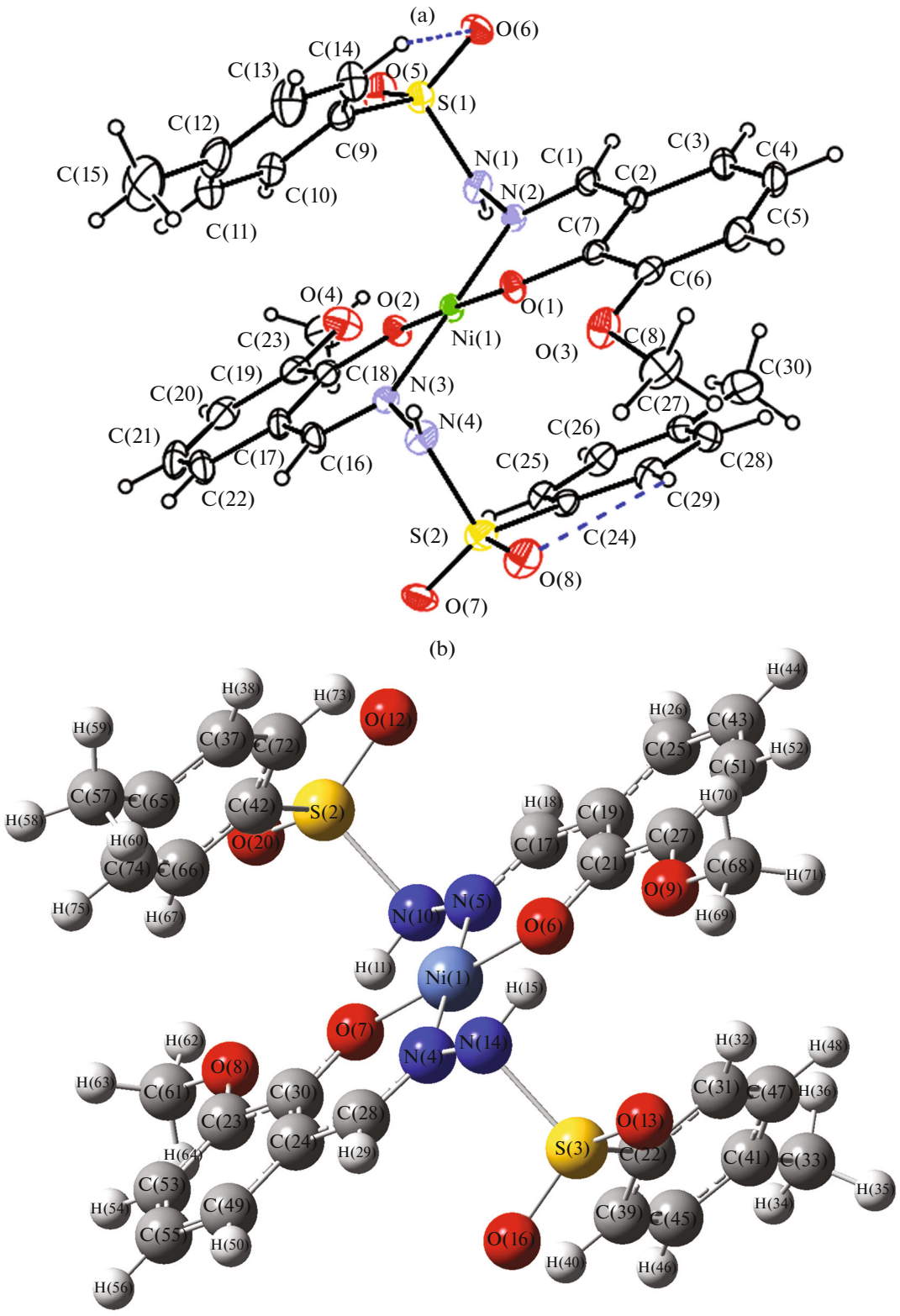

Fig. 1. ORTEP III drawing of the basic crystallographic unit of the title compound, showing the atom-numbering scheme (a) (displacement ellipsoids are drawn at the 20% probability level and all H atoms are shown as small spheres of arbitrary radii); Gaussian 03 view drawing of **I** (b).

Table 3. Geometric parameters of hydrogen bonds of **I***

D–H···A	Distance, Å			D–H···A/Cg, deg
	D–H	H···A/Cg	D···A/Cg	
C(14)–H(14)···O(6)	0.93	2.54	2.908(6)	104
C(29)–H(29)···O(8)	0.93	2.59	2.946(6)	103
C(3)–H(3)···O(8)[i]	0.93	2.52	3.262(6)	137
C(14)–H(14)···Cg(5)[ii]	0.93	2.89	3.756(5)	155
C(21)–H(21)···Cg(3)[iii]	0.93	2.86	3.627(5)	140

* Symmetry codes: [i] $1 + x, y, z$; [ii] $1/2 + x, 1/2 - y, 1/2 + z$; [iii] $-1/2 + x, 1/2 - y, -1/2 + z$; Cg(3) centroid of (C(2)–C(7)) ring, Cg(5) centroid of (C(17)–C(22)) ring.

Table 4. Vibrational frequencies of **I** with experimental and DFT/B3LYP methods

Frequencies	Experimental	B3LYP/3-21G	B3LYP/6-311G
ν (CH) aromatic		3250–3230	3217–3207
ν_{as}(CH) aromatic		3216/3201	3192/3178
ν_{as}(CH)		3212	3188
$\nu_{as}(CH_3)$	2975	3182–3096	3163–3077
ν(NH)	3101	3059	3202
$\nu(CH_3)$ + ν(NH)		3051–3035	3017–3007
ν(CC)		1635	1643
ν(CC) + δ(NH) + ν(C=N)	1610	1600	1608/1574
$\delta(CH_3)$		1571	1536
$\rho_t(CH_3)$ + δ(CH) + δ(NH)		1566–1557	1530
δ(CH) aromatic	1544	1545/1512/1482	1517/1494
δ(NH)	1470	1533/1512/1474	1526/1494
$w(CH_3)$	1451	1492/1474	1494
ρ_s(CH)	1461/1367	1446/1237	1485/1362
ν(CC) + δ(NH) + δ(CH) + δ(CCO) + δ(CCN)	1358	1360	1467
ν(CO) linked methyl	1293	1272	1377–1362
ν(CO) + ν(CN)	1320	1474	1342
θ(Phenyl)	1251	1225–1107	1277
ρ_t(NH) + ν(SO)	1117	1177/1079	1362/1148
ρ_s(CH) aromatic	1226/1183		1226/1154
t(CH) aromatic	1088–1104	1047–1018	1010
ν(NN)	1031	994	1021
t(CH)	962	965	990/973
ν_{as}(OSO)	1166	1094/1079	887
w(CH) aromatic	774/902	887/783	834/793
ν(ONiO)	568	919/777	826
δ(ONiO)		727	
ν(NNiN)	445	669	
δ(NNC)	745		767
ν(OSO)	1318	903	748

ρ_t—rocking, *t*—twist, δ—bending, ρ_s—scissorsing,: ν_s—symmetric stretching, ν_{as}—asymmetric stretching, θ—breathing.

Table 5. MO energies of **I** with DFT method

Energies	B3LYP/3-21G	B3LYP/6-311G
HOMO, a.u.	–0.183	–0.211
LUMO, a.u.	–0.075	–0.108
Δ, a.u. (eV)	0.108(2.939)	0.103(2.803)
Total energies, a.u.	–4264.468	–4286.320
Dipole moment, Debye	0.224	0.087

1 a.u. = 27.2116 eV.

$\nu_{as}(SO_2)$ vibrations. These values are in accord with reported structure in [32]. In additional to these, the calculated vibrational frequencies can be seen in Table 4. In general, when the calculated IR frequencies are compared with the experimental data of **I**, approximately all data agree with calculated vibrations. Because experimental results are solid phase and theoretical calculations are gaseous phase, there is a minor difference between the data.

MEP is related to electron density and is a very useful descriptor in understanding sites for electrophilic (electron-deficient, positively charged species) attack and nucleophilic (an electron rich, negatively charged species) reactions as well as hydrogen-bonding interactions [36]. To predict reactive sites for electrophilic attack for **I**, MEP was calculated at the B3LYP/3-21G optimized geometry. The negative regions of MEP were related to electrophilic reactivity and the positive ones to nucleophilic reactivity (Fig. 3). This molecule has a possible site for electrophilic attack. The negative regions are mainly over oxygen atoms with O(5), O(6), O(7), and O(8) atoms. Total density, contour of total density, alpha density, electrostatic potential, the contour of electrostatic potential and molecular electrostatic potential are shown in Fig. 3.

The calculations indicate that **I** has 181 occupied molecular orbitals (MOs). The HOMO energies, the LUMO energies, and the energy gaps are given in Table 5. The frontier MOs play an important role in electrical and optical properties, as well as in UV-Vis spectra and chemical reactions [37]. Based on the B3LYP/3-21G and B3LYP/6-311G optimized geometries, the total energy of I has been calculated by these methods, as –4264.468 and –4286.320 a.u., respectively. An electronic system with a larger HOMO–LUMO gap should be less reactive than one having a

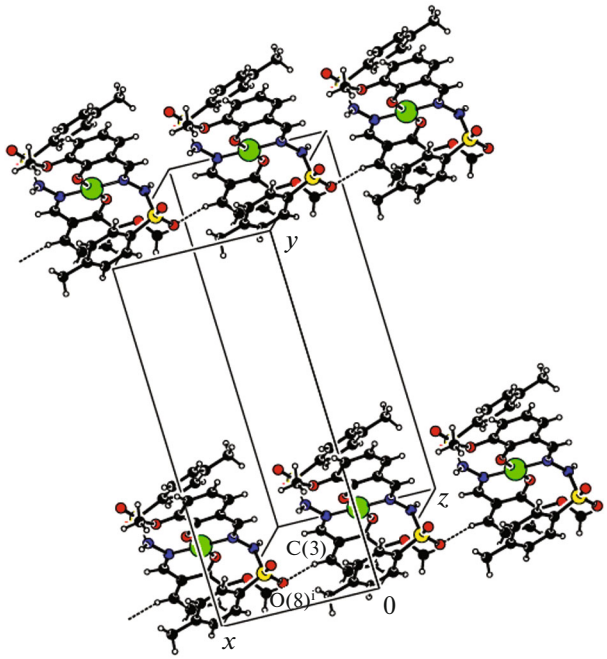

Fig. 2. Intermolecular C(3)–H(3)···O(8) hydrogen bonding extending along *x*. Symmetry code: 1 + *x*, *y*, *z*.

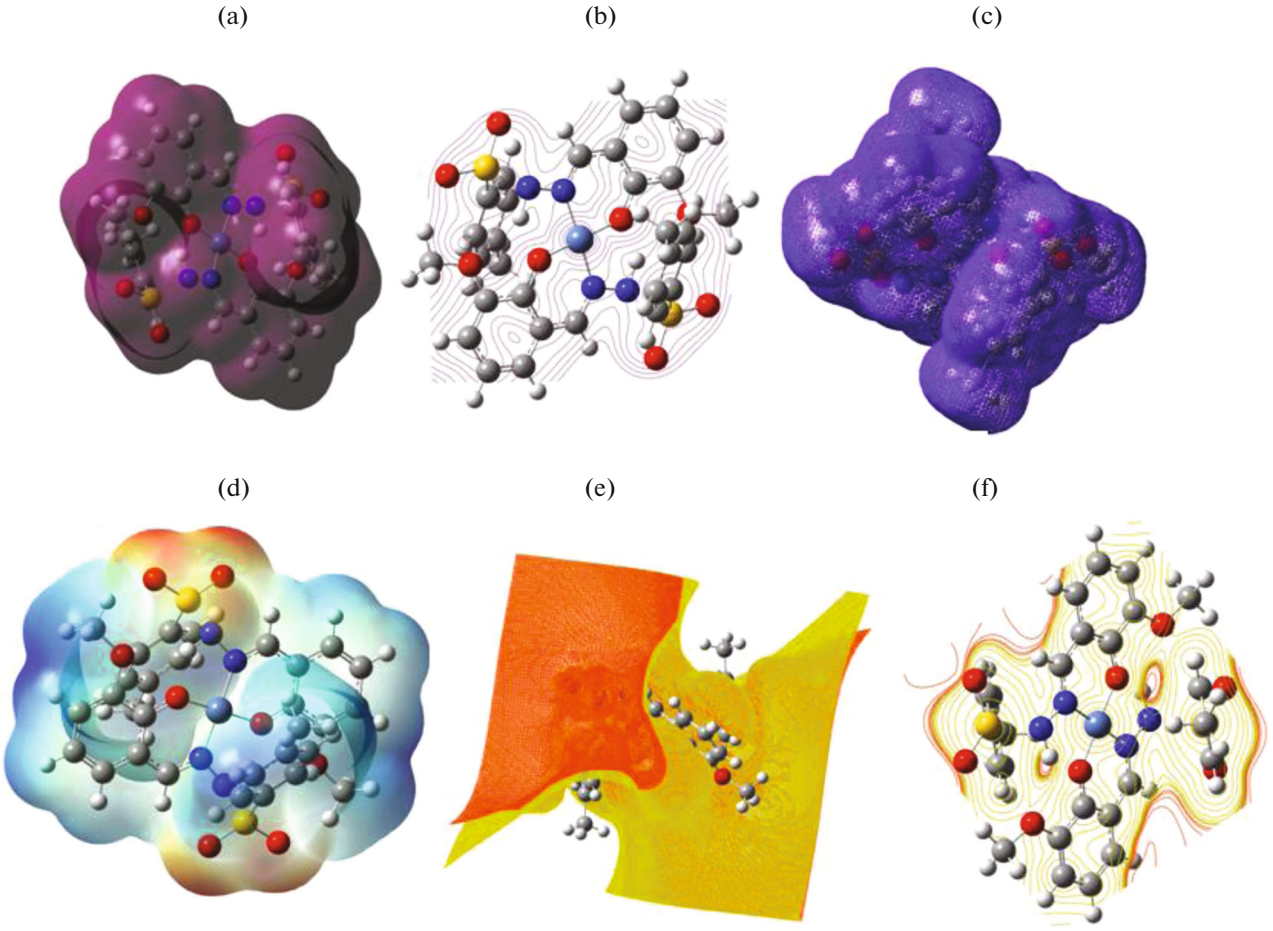

Fig. 3. (a) total density, (b) contour (total density), (c) alpha density, (d) MEP, (e) ESP, (f) contour (ESP) map (in a.u.) of **I** with the TDDFT/B3LYP/3-21G method (with an isodensity value of 0.0004 a.u.).

smaller gap [38]. In this study, the HOMO–LUMO gaps (Fig. 4) of the molecule are at 2.939 eV (λ = 423 nm) and 2.803 eV (λ = 444 nm) for the B3LYP/3-21G and B3LYP/6-311G methods, respectively (Table 5), and this energy gap indicates that the structure is very stable.

Besides of these properties of the molecule, we have calculated ionization potential, electron affinity, electronegativity, chemical hardness and chemical softness of the molecule with DFT. The energy HOMO is sometimes considered as an approximation to the ionization potential while the energy LUMO is considered as an approximation to the electron affinity. The ionization potentials (I = –HOMO) of the molecule are 4.980 and 5.742 eV for B3LYP/3-21G and B3LYP/6-311G basis sets, respectively. The electron affinity (A = –LUMO) of the molecule are 2.041 and 2.939 eV for B3LYP/3-21G and B3LYP/6-311G basis sets, respectively. The electronegativity ($\psi = (I + A)/2$) of the molecule are 3.510 and 4.340 eV for B3LYP/3-21G and B3LYP/6-311G basis sets, respectively. The chemical hardness ($\eta = (I - A)/2$) of the molecule are 1.469 and 1.401 eV for B3LYP/3-21G and B3LYP/6-311G basis sets, respectively. The chemical softness ($s = 1/2\eta$) of the molecule are 0.340 and 0.357 eV for B3LYP/3-21G and B3LYP/6-311G basis sets, respectively.

The experimental UV-Vis spectrum of complex **I** is complicated by the presence of intense absorption 253 and 336 nm due to the Schiff base ligand. The absorption bands 253 and 336 nm can be assigned to $\pi \rightarrow \pi^*$ and $n \rightarrow \pi^*$ transitions of the ligand. There is two absorption bands at 430 and 618 nm in the spectrum of complex **I**. The first band of relatively high intensity is assigned as ligand → metal charge transfer transition. These cond weak band corresponds to the $d \rightarrow d$ transitions. It is seen that the wavelengths of HOMO–LUMO gap calculated by using B3LYP/3-21G and

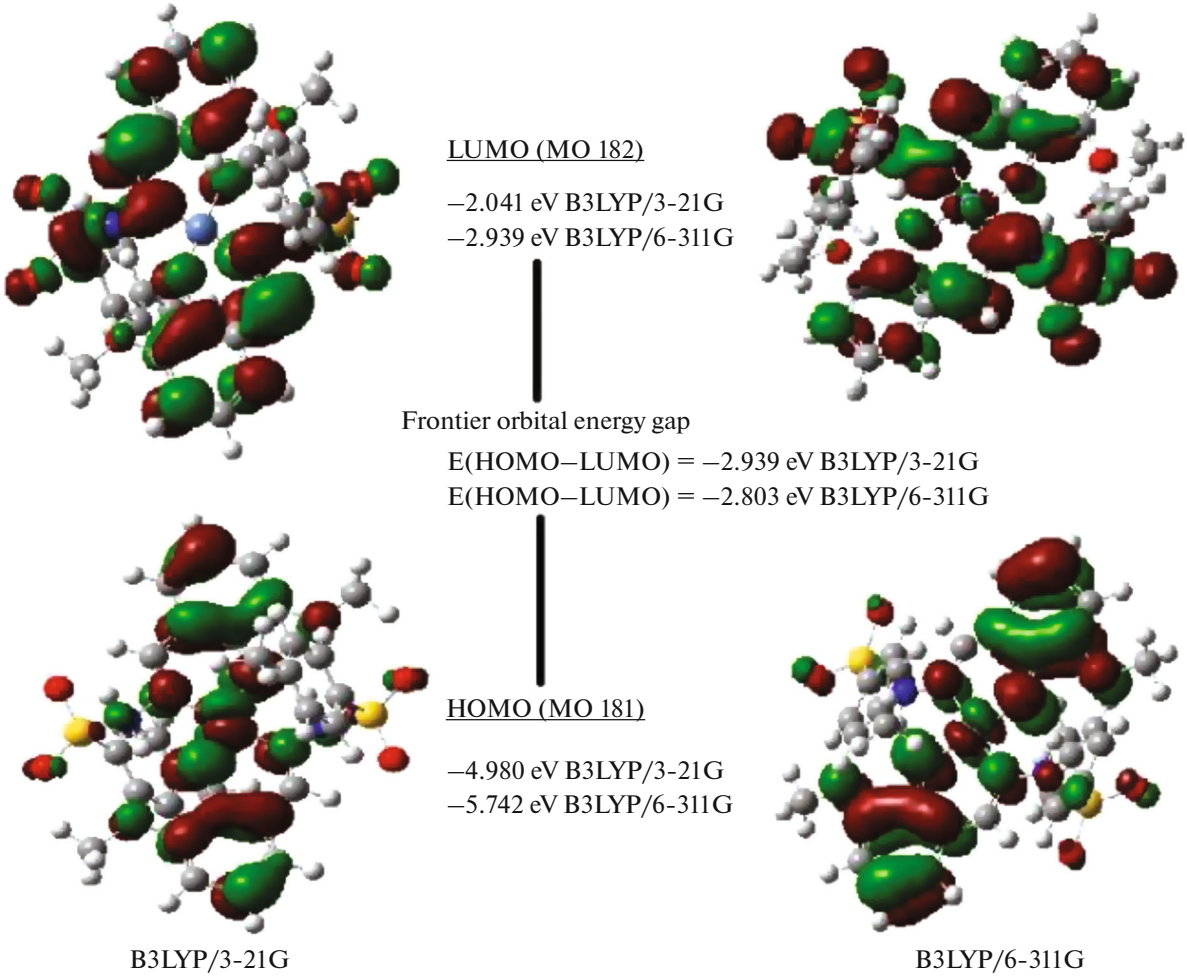

Fig. 4. Patterns of the HOMO, LUMO of **I** obtained with TDDFT/B3LYP/3-21G and B3LYP/6-311G methods.

B3LYP/6-311G methods agreeable experimentally ligand → metal charge transfer transition.

The magnetic susceptibility measurement of I indicates diamagnetism.

REFERENCES

1. Şenyüz, N., Yüksektepe, Ç., Batl, H.R., et al., *Acta Crystallogr., Sect. E: Struct. Rep. Online*, 2006, vol. 62, p. m3163.
2. Tarafder, M.T.H., Jin, K.T., Crouse, K.A., et al., *Polyhedron*, 2002, vol. 21, p. 2547.
3. Guerriero, P., Tamburini, S., and Vigato, P.A., *Coord. Chem. Rev.*, 1995, vol. 139, p. 17.
4. Sreekala, R. and Yusuf, K.K.M., *React. Kinet. Catal. Lett.*, 1992, vol. 48, p. 575.
5. Das, N.N. and Dash, A.C., *Polyhedron*, 1995, vol. 14, p. 1221.
6. Williams, D.R., *Chem. Rev.*, 1972, vol. 72, p. 203.
7. Babahan, I., Coban, E.P., and Bıyık, H., *Maejo Int. J. Sci. Techno.*, 2013, vol. 7, p. 26.
8. Assayehegn, E., *Thesis*, Addis Ababa Uiversity School of Graduate Studies, Department of Chemistry Graduate Program, August, 2007.
9. Kumar, M. and Saxena, P.N., *Ori. J. Chem.*, 2012, vol. 28, no. 4, p. 1927.
10. Armbruster, F., Klingebiel, U., and Noltemeyer, M., *Z. Naturforsch., B: J. Chem. Sci.,* 2006, vol. 61, p. 225.
11. Senturk, O.S., Sert, S., and Ozdemir, U., *Z. Naturforsch., B: J. Chem. Sci.,* 2003, vol. 58, p. 1124.
12. Amr, A.E.G.E., Mohamed, A.M., and Ibrahim, A.A., *Z. Naturforsch., B: J. Chem. Sci.,* 2003, vol. 58, p. 861.
13. Mohrle, H. and Keller, G., *Z. Naturforsch., B: J. Chem. Sci.,* 2003, vol. 58, p. 885.
14. Chakraborty, J., Singh, R.K.B., Samanta, B., et al., *Z. Naturforsch., B: J. Chem. Sci.,* 2006, vol. 61, p. 1209.
15. Lozan, V., Lassahn, P.-G., Zhang, C., et al., *Z. Naturforsch., B: J. Chem. Sci.,* 2003, vol. 58, p. 1152.
16. Zeyrek, C.T., Elmali, A., and Elerman, Y., *Z. Naturforsch., B: J. Chem. Sci.,* 2006, vol. 61, p. 237.

17. Dey, D.K., Samanta, B., Lycka, A., and Dahlenburg, L., *Z. Naturforsch., B: J. Chem. Sci.,* 2003, vol. 58, p. 336.
18. Janiak, C., Lassahn, P.-G., and Lozan, V., *Macromol. Symp.*, 2006, vol. 236, p. 88.
19. Katyal, M. and Dutt, Y., *Talanta*, 1975, vol. 22, p. 151.
20. Mohan, M., Gupta, M.P., Chandra, L., and Jha, N.K., *Inorg. Chim. Acta*, 1988, vol. 151, p. 61.
21. Sinh, R.B. and Jain, P., *Talanta*, 1982, vol. 29, p. 77.
22. Suez, I., Pehkonen, S.O., and Hoffmann, M.R., *Sci. Technol.*, 1994, vol. 28, p. 2080.
23. Terra, L.H., Areias, A.M.C., Gaubeur, I., and Suez-Iha, M.E.V., *Spectrosc. Lett.*, 1999, vol. 32, p. 257.
24. Becke, A.D., *J. Chem. Phys.*, 1993, vol. 98, p. 5648.
25. Lee, C., Yang, W., and Parr, R.G., *Phys. Rev. B: Condens. Matter Mater. Phys.*, 1988, vol. 37, p. 785.
26. Frish, A., Nielseni, A.B., and Holder, A.J., *Gaussview User Manual*, Pittsburg (PA): Gaussian Inc., 2001.
27. Frischm, M.J., Trucksm, G.W., Schlegelm, H.B., et al., *Gaussian 03*, Wallingford (CT): Gaussian, Inc., 2004.
28. Sheldrick, G.M., *SHELXS-97 and SHELXL-97*, Göttingen (Germany): Univ. of Göttingen, 1997.
29. Farrugia, L.J., *J. Appl. Crystallogr.*, 1999, vol. 30, p. 837.
30. *Oxford Diffraction. CrysAlis PRO,* Abingdon (England): Oxford Diffraction Ltd., 2007.
31. Farrugia, L.J., *J. Appl. Crystallogr.*, 1997, vol. 30, p. 565.
32. Şenyüz, N., Ataol, Ç.Y., and Batl, H.R., *J. Coord. Chem.*, 2014, vol. 40, no. 11, p. 849.
33. Allen, F.H., Kennard, O., Watson, D.G., et al., *Perkin Trans.*, 1987, vol. 2, p. 1.
34. Koz, G., Özdemir, N., Astley, D., et al., *J. Mol. Struct.*, 2010, vol. 966, p. 39.
35. Bernstein, J., Davis, R.E., Shimoni, L., and Chang, N.L., *Angew. Chem. Int. Ed.*, 1995, vol. 34, p. 1555.
36. Yüksektepe, Ç., Saraçoğlu, H., Çalışkan, N., et al., *Bull. Korean Chem. Soc.*, 2010, vol. 31, p. 3553.
37. Fleming, I., *Frontier Orbitals and Organic Chemical Reactions,* London: Wiley, 1976.
38. Kurtaran, R., Odabaşoğlu, S., Azizoğlu, A., et al., *Polyhedron,* 2007, vol. 26, p. 5069.